Crystal Structure of *allo*-Ile^{A2}-Insulin, an Inactive Chiral Analogue: Implications for the Mechanism of Receptor Binding[†,‡]

Zhu-li Wan,[§] Bin Xu,[§] Ying-Chi Chu,[||] Panayotis G. Katsoyannis,[||] and Michael A. Weiss*[,§]

Department of Biochemistry, Case Western Reserve University School of Medicine, Cleveland, Ohio 44106, and Department of Pharmacology and Biological Chemistry, Mt. Sinai School of Medicine of New York University, New York, New York 10029

Received March 18, 2003; Revised Manuscript Received September 9, 2003

ABSTRACT: The crystal structure of an inactive chiral analogue of insulin containing nonstandard substitution *allo*-Ile^{A2} is described at 2.0 Å resolution. In native insulin, the invariant Ile^{A2} side chain anchors the N-terminal α-helix of the A-chain to the hydrophobic core. The structure of the variant protein was determined by molecular replacement as a T_3R_3 zinc hexamer. Whereas respective T- and R-state main-chain structures are similar to those of native insulin (main-chain root-mean-square deviations (RMSD) of 0.45 and 0.54 Å, respectively), differences in core packing are observed near the variant side chain. The R-state core resembles that of the native R-state with a local inversion of A2 orientation (core side chain RMSD 0.75 Å excluding A2); in the T-state, *allo*-Ile^{A2} exhibits an altered conformation in association with the reorganization of the surrounding side chains (RMSD 0.98 Å). Surprisingly, the core of the R-state is similar to that observed in solution nuclear magnetic resonance (NMR) studies of an engineered T-like monomer containing the same chiral substitution (*allo*-Ile^{A2}-DKP-insulin; Xu, B., Hua, Q. X., Nakagawa, S. H., Jia, W., Chu, Y. C., Katsoyannis, P. G., and Weiss, M. A. (2002) *J. Mol. Biol. 316*, 435−441). Simulation of NOESY spectra based on crystallographic protomers enables the analysis of similarities and differences in solution. The different responses of the T- and R-state cores to chiral perturbation illustrates both their intrinsic plasticity and constraints imposed by hexamer assembly. Although variant T- and R-protomers retain nativelike protein surfaces, the receptor-binding activity of *allo*-Ile^{A2}-insulin is low (2% relative to native insulin). This seeming paradox suggests that insulin undergoes a change in conformation to expose Ile^{A2} at the hormone−receptor interface.

Insulin is a globular protein containing two chains, designated A (21 residues) and B (30 residues). Stored in the β−cell as a Zn^{2+}-stabilized hexamer, the hormone functions as a Zn^{2+}-free monomer (*1*). The structure of a monomer in solution (*2*−*4*) resembles the crystallographic T-state as defined in a variety of crystal forms (*5*−*11*). The present study focuses on the structural role of Ile^{A2}, an invariant side chain in the core (*12*, *13*). Ile^{A2} anchors the A1-A8 α-helix through a network of long-range contacts involving Cys^{A6} (part of the internal A6-A11 disulfide bridge), Leu^{A16}, Tyr^{A19}, Leu^{B6}, Leu^{B11}, and Leu^{B15}. Reorganization of the B-chain on receptor binding is proposed to expose Ile^{A2} to engage the insulin receptor (*2*, *13*, *14*). In this paper, we describe the crystal structure of an insulin analogue in which Ile^{A2} is substituted by *allo*-Ile^{A2}. Previous studies have demonstrated that such chiral inversion impairs insulin's activity by 50-fold (*13*, *15*). The structure is determined as a $T_3R^f_3$ zinc hexamer and so defines the consequences of the nonstandard substitution in two contexts, T- and R-state protomers (Figure 1).[1] Our results are compared to those of a recent NMR[2] study of an engineered monomer DKP-insulin (*16*) containing the same substitution (*15*).[3]

Anomalies encountered in studies of structure−function relationships suggest that insulin's B-chain undergoes a change in conformation on receptor binding. An inactive

[†] This work was supported in part by grants from the National Institutes of Health to P.G.K. (DK 56673) and M.A.W. (DK 40949).

[‡] Coordinates have been deposited in the Protein Databank (accession code 1Q4V).

* To whom correspondence should be addressed. E-mail: weiss@biochemistry.cwru.edu. Tel: (216) 368-5991. Fax: (216) 368-3419.

[§] Case Western Reserve University School of Medicine.

[||] Mt. Sinai School of Medicine of New York University.

[1] The crystallographic T → R transition, an allosteric reorganization of insulin hexamers (*6*, *24*), is remarkable for a change in the secondary structure of the B1-B8 segment from extended (T-state) to α-helix (R-state). Segmental reorganization is coupled to a change in conformation of Gly^{B8}, nonlocal features of core packing, and handedness of cystine A7-B7. The latter sulfur atoms are exposed in the T-state but buried in a nonpolar crevice in the R-state. The superscript R^f refers to N-terminal fraying of the B1-B19 α-helix (*10*).

[2] Abbreviations: CD, circular dichroism; DG, distance geometry; DPI, *des*-pentapeptide[B26-B30]-insulin; NMR, nuclear magnetic resonance; NOEs, nuclear Overhauser enhancements; NOESY, NOE spectroscopy; RMD, restrained molecular dynamics; RMS, root-mean-square; RMSD, RMS deviations; SA, simulated annealing. Amino acids are represented by standard one- and three-letter codes. Native elements of structure designate features of crystal structures and may not correspond to the functional conformation in a hormone−receptor complex.

[3] DKP-insulin, an engineered insulin monomer of high activity (*16*), contains three substitutions in the B-chain: His^{B10} → Asp, Pro^{B28} → Lys, and Lys^{B29} → Pro. The latter two influence the structure of the C-terminal β-strand of the B-chain and its potential interactions with the N-terminal region of the A-chain, including Ile^{A2} (*44*). For this reason, it is of interest to investigate effects of the *allo*-Ile^{A2} inversion in an otherwise native context.

10.1021/bi034430o CCC: $25.00
Published on Web 10/16/2003

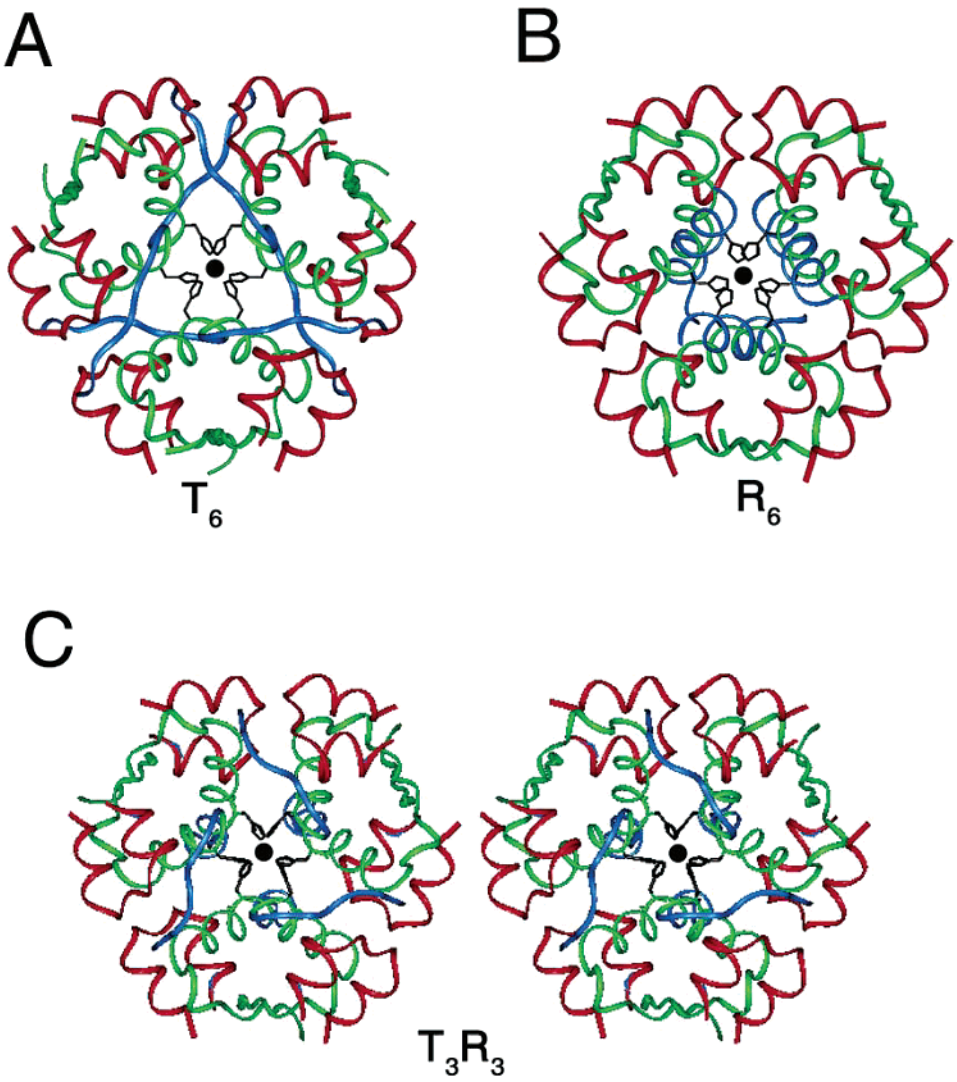

FIGURE 1: Crystal structures of insulin. (A) Ribbon representation of 2-Zn insulin hexamer (T_6). Zinc ion is shown as black sphere coordinated by histidine side chains. A-chains are shown in red and B-chains in blue (residues B1-B8) or green (B9-B30). (B) Corresponding ribbon representation of phenol-stabilized hexamer (R_6). (C) Stereoview of T_3R_3 hexamer of *allo*-Ile^{A2}-insulin described herein; coloring scheme as in panel A.

single-chain analogue, mini-proinsulin, exhibits an essentially native crystal structure (*14*). Mini-proinsulin contains a peptide bond between Lys^{B29} and Gly^{A1}, which constrains the relative orientation of the B-chain's C-terminal β-strand and α-helical core. We and others have proposed that the B-chain's C-terminal β-strand detaches on receptor binding (*2*, *14*). This model rationalizes effects of C-terminal B-chain substitutions and deletions on receptor binding (*2*, *17*, *18*). Effects of such detachment on insulin's structure and surface have been investigated through crystallographic studies of a truncated insulin analogue (*des*-pentapeptide[B26-B30]-insulin (DPI); refs *7*, *8*, and *19*). When amidated at B25, DPI exhibits wild-type activity (*20*, *21*). The crystal structure of DPI (*7*, *8*, *19*) exhibits a native α-helical subdomain; the absence of residues B26-B30 leads to significant exposure of core side chains Ile^{A2} and Val^{A3}. Detachment or reorganization of the B-chain β-strand on receptor binding would likewise expose Ile^{A2} and Val^{A3} as part of a putative hidden functional surface (*2*, *14*, *22*). The extent of structural reorganization of the B23-B30 segment on receptor binding is not well-characterized (*23*). Further, because additional conformational changes may occur elsewhere in the B-chain (*24*), the detachment model may underestimate the extent of induced fit. Unlike the B-chain, the A-chain is thought to function as a preformed recognition element (*4*, *9*, *25*, *26*).

The contribution of individual side chains to insulin's biological activity has been investigated by alanine scanning mutagenesis (*27*). Substitution of Ile^{A2} by alanine impairs biological activity by 200-fold (*12*, *13*), an unusually severe decrement among mutant insulins (*9*). Interpretation of this result is unclear, however, as an NMR study of an Ala^{A2} analogue demonstrated segmental destabilization of the N-terminal A-chain α-helix (*28*). Such nonlocal perturbations are avoided by the substitution of Ile^{A2} by *allo*-Ile^{A2} (*15*), which preserves side-chain volume and hydrophobicity. An NMR study of an analogue containing *allo*-Ile^{A2} and three B-chain substitutions demonstrated maintenance of a native-like structure (*15*). Because of the limitations of solution structures of insulin analogues (they are ordinarily less well-defined than crystal structures, contain additional substitutions designed to prevent self-association, and often include data obtained under nonphysiological conditions[4]), we sought to obtain a crystal structure of *allo*-Ile^{A2}-insulin. Crystallography offers the advantages of high resolution and cross

validation, but its interpretation can sometimes be constrained by effects of protein assembly. Comparison of NMR and crystallographic results thus promises an integrated approach to analysis of structure−function relationships.

In this paper, we describe the crystal structure of *allo*-Ile^{A2}-insulin at a resolution of 2.0 Å and analyze its relationship to an ensemble of solution structures. The crystal structure defines how T- and R-state protomers accommodate the inversion of A2 side-chain chirality in their cores. These accommodations are inequivalent, reflecting the plasticity of packing schemes seen among different crystal forms of native insulin (*5*, *6*, *24*). Surprisingly, the conformation of *allo*-Ile^{A2} in an engineered T-like monomer in solution (*15*) resembles that observed in the crystallographic R-state, an allosteric product of hexamer assembly (*6*, *24*). Comparison of the observed NMR spectrum with simulated spectra calculated on the basis of the crystallographic protomers reveals that the engineered monomer, although T-like in secondary structure, in part exhibits nuclear Overhauser enhancements (NOEs) between core side chains more consistent with the R-state. These observations support the view that the conformational repertoire of an insulin monomer spans the range of diverse crystal forms (*29*). The crystal structure of *allo*-Ile^{A2}-insulin further demonstrates that the nonstandard substitution does not perturb the surface of the protein, including side chains involved in self-association (*9*) and/or proposed to contact the insulin receptor (*9*, *25*, *30*, *31*). We propose that stereospecific recognition of Ile^{A2} by the insulin receptor is coupled to detachment of the C-terminal B-chain β-strand and reorganization of the hormone's hydrophobic core.

MATERIALS AND METHODS

Peptide Synthesis and Chain Combination. An *allo*-Ile^{A2} analogue of the human insulin A-chain was prepared by solid-phase chemical synthesis, modified to form the tetra-*S*-sulfonate derivative, and combined with the native B-chain-di-*S*-sulfonate as described (*32*). Efficiency of chain combination was not affected by the substitution. The molecular weight of the analogue was found by mass spectrometry to be the same as that of human insulin.

Biological Assays. Receptor-binding studies were performed using a human placental membrane preparation as described (*32*). Relative activity is defined as the ratio of analogue to human insulin required to displace 50% of specifically bound ^{125}I-human insulin (purchased from Amersham).

Crystallization Conditions. Crystals were grown by hanging-drop vapor diffusion in the presence of a 1:2.5 ratio of Zn^{2+} to protein monomer and a 3.7:1 ratio of phenol to protein monomer in Tris-HCl buffer. Drops consisted of 2 μL of protein solution (10 mg/mL in 0.02 M HCl) mixed with 2 μL of reservoir solution (0.02 M Tris-HCl, 0.05 M sodium citrate, 5% acetone, 0.03% phenol, and 0.01% zinc acetate at pH 8.0). Each drop was suspended over 1 mL of reservoir solution. Crystals were obtained at room temperature after two weeks. Phenol was found to be essential for the crystallization of *allo*-Ile^{A2}-insulin; in its absence, the protein formed a glassy precipitate even in the presence of zinc ions. Chloride ion was by contrast not necessary.

X-ray Diffraction and Data Collection. Data were collected from single crystals of *allo*-Ile^{A2}-insulin mounted in a capillary. A 23.2−2.0 Å data set (obtained from two crystals) was collected at room temperature using an R-AXIS IV imaging-plate system mounted on Rigaku RU 200 rotating anode generator with CuKα radiation. Diffraction was measured at a crystal-to-detector distance of 100 mm. Intensity data were recorded using an oscillation angle of 1.5° in 120 frames, giving a total of 180° of data. Data were processed with programs DENZO (version 1.9.6) and SCALEPACK (version 1.9.6). Crystals belong to space group R3 with hexagonal unit cell dimensions $a = b = 80.49$ Å and $c = 37.94$ Å. The data set consisted of 5892 unique reflections merged from 12 199 independent observations. The R_{merge} value was 0.057. Ten percent of the reflections were excluded from the refinement to provide an estimate of the free (cross-validated) R value (*33*).

Molecular Replacement and Refinement. The structure was determined by molecular replacement using CNS (*34*). The dimensions of the unit cell are characteristic of a $T_3R^f_3$ hexamer in a lattice similar to that of rhombohedral 4-Zn insulin (*10*). Cell dimensions imply one dimer per asymmetric unit in accord with past studies of this crystal form. The dimensions of the unit cell in themselves suggest the presence of a $T_3R^f_3$ hexamer as T_6 and R_6 crystals are associated with different unit cell dimensions (T_6: $a = 82.5$ Å and $c = 34.0$ Å; R_6: $a = 62.3$ Å, $b = 61.8$ Å, and $c = 47.8$ Å; $\alpha = 90°$, $\beta = 110.7°$, and $\gamma = 90°$; rhombohedral R_6: $a = 78.86$ Å and $c = 39.5$ Å). Accordingly, a model was obtained by molecular replacement using the native TR dimer (PDB code 1TRZ following removal of all water molecules and zinc and chloride ions). The position of the dimer in the asymmetric unit was defined by rotation−translation search; the quality of the solution was verified by the correlation coefficient (0.398) and initial R factor (45.9%). A trial model (with Ile^{A2} substituted by glycine and B-chain residues B1-B9 of molecule 2 excluded) was refined by restrained molecular dynamics. At subsequent stages, *allo*-Ile^{A2} and residues B1-B9 of molecule 2 were built into the density (intermediate R factor 32.9%). Between refinement cycles, $2F_o - F_c$ and $F_o - F_c$ maps were calculated using data to 3.0 Å resolution; a phenol molecule was built into the structure using the program O (*35*). The geometry was continually monitored with PROCHECK (*36*), and zinc ions and water molecules were built into the difference map as the refinement proceeded. Conformations of *allo*-Ile^{A2} and neighboring residues in each protomer were verified in an omit map calculated from a model in which residues A1-A8 were deleted. Calculation of omit maps and further refinement were carried out using CNS (*34*) and X-PLOR (*37*) programs, which implement maximum-likelihood torsion-angle dynamics, conjugate-gradient refinement, an overall bulk solvent correction, and anisotropic temperature factor correction. Bond distances between zinc ions and N$^{\epsilon 2}$ of the His^{B10} residues were unrestrained. Representative

[4] Although high-quality NMR spectra of monomeric insulin analogues are readily obtained in D_2O at pH 7−8, corresponding spectra in H_2O (*3*, *4*) are incomplete due to base-catalyzed amide protein exchange and conformational broadening of amide resonances. To circumvent this, supplemental spectra are often obtained at pH 2−3 or in 20% acetic acid. Distance geometry models typically include restraints obtained from both sets of conditions (*4*, *15*).

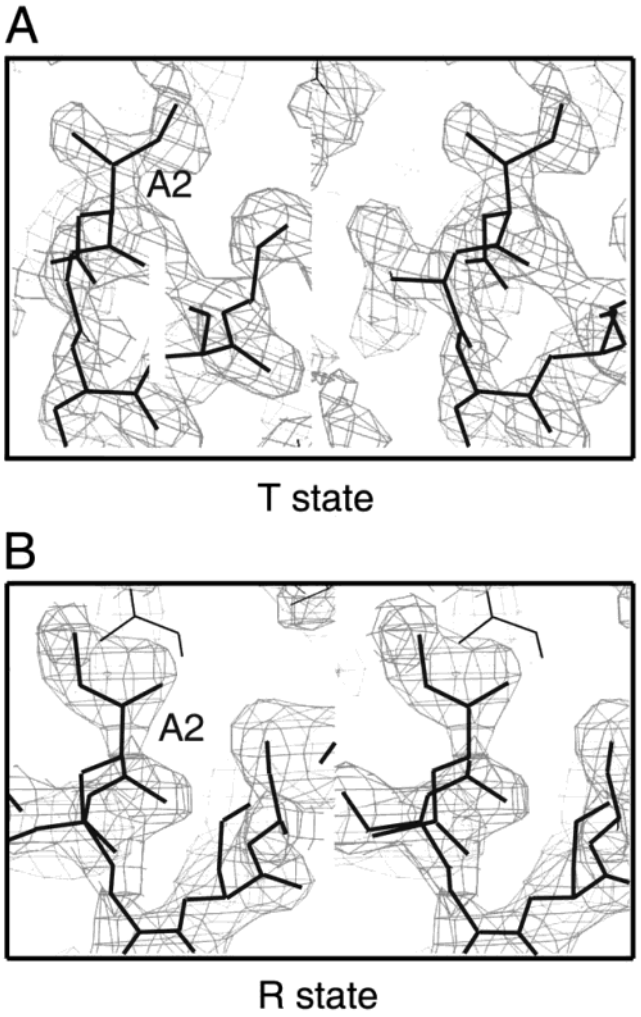

FIGURE 2: Electron density and atomic positions of residues of A1-A5 in *allo*-Ile^{A2}-insulin: (A) $2F_o - F_c$ electron density map of molecule 1 (T-state) and (B) corresponding region in R-state. Maps are contoured at 1.0 σ using program O.

electron density depicting *allo*-Ile^{A2} and neighboring residues in molecules 1 and 2 in a ($2F_o - F_c$) Fourier map are shown in Figure 2. After refinement, the final model consisted of 810 protein atoms (i.e., the TR^f dimer in the asymmetric unit), one phenol molecule, two zinc ions, and 64 water molecules. The refined model yielded an *R* factor of 0.219 and a free *R* factor of 0.264 for all measured data (23.2−2.0 Å). Zinc ion coordination distances to N$^{\epsilon 2}$ of His^{B10} residues were 1.99 Å (T-state) and 2.08 Å (R-state). Distances between water molecules and the protein are in the range of 2.7−3.4 Å. RMS deviations from standard geometry and refinement statistics are given in Table 2.

Circular Dichroism (CD). Spectra were obtained using an Aviv spectropolarimenter. Samples were placed in a 1 mm path length quartz cuvette for wavelength scans and a 1 cm quartz cuvette for guanidine denaturation studies. Spectra were obtained in 0.01 M HCl (pH 2.0) or under neutral conditions (50 mM KCl and 10 mM potassium phosphate; pH 7.0). CD-detected guanidine unfolding curves at 222 nm were obtained in 50 mM KCl and 10 mM potassium phosphate (pH 7.0) at 4 °C with automated titration unit as described (*26*). The protein concentration in guanidine studies was 5 μM.

Table 1: Activity and Thermodynamic Stability[a]

analogue	activity	ΔG_u	$\Delta\Delta G_u$	C_{mid} (M)	*m* (kcal/mol/M)
native insulin	100	3.3 ± 0.1		4.8 ± 0.1	0.69 ± 0.01
allo-Ile^{A2}-insulin	2	3.2 ± 0.1	0.1 ± 0.2	5.2 ± 0.2	0.61 ± 0.01

[a] ΔG_u indicates the apparent change in free energy on denaturation in guanidine-HCl as extrapolated to zero denaturant concentration by a two-state model (*38*). $\Delta\Delta G_u$ indicates a difference in the ΔG_u values. Uncertainties in two-state fitting parameters do not include possible systematic errors due to non-two-state behavior. C_{mid} is defined as that concentration of guanidine-HCl at which 50% of the protein is unfolded. The *m* value provides a slope in plotting the unfolding free energy ΔG_u ([G_u·HCl]) vs molar concentration of denaturant.

Table 2: X-ray Diffraction and Refinement Statistics

resolution limits (Å)	23.2−2.0
R value	0.219
R_{free} value	0.264
R_{merge}	
all data	0.057
overall $I/\sigma(I)$	43.1
highest resolution shell	0.301
$I/\sigma(I)$	4.1
Overall	
reflections used	5892
completeness (%)	98.7
data redundancy	2.07
protein atoms	810
water molecules	64
Highest Resolution Shell	
resolution range (Å)	2.07−2.0
no. of reflections	543
completeness (%)	89.3
data redundancy	1.27
R value	0.331
R_{free} value	0.378
RMSD from Standard Geometry	
bond lengths (Å)	0.010
bond angles (deg)	2.1
dihedral angles (deg)	24.1
improper angles (deg)	0.90
average *B* factor	29.52
protein	29.14
solvent	33.83
Cross-Variations from Estimated Error	
ESD from C-V Luzzati plot	0.20
ESD from C-V σ	0.25
Ramachandran Plot	
no. of residues in most-favored region (%)	91.9
additional allowed region (%)	8.1
Isotropic Thermal Model Restraints (Å^2)	
main-chain bonds	1.41
main-chain angles	2.05
side-chain bonds	2.47
side-chain angles	3.10

Thermodynamic Modeling. Guanidine denaturation data were fitted by nonlinear least squares to a two-state model (*38*). CD data $\theta(x)$, where *x* indicates the concentration of denaturant, were fitted by a nonlinear least-squares program to yield estimates of ΔG_u, C_{mid}, and *m* as described (see Table 1; ref *32*). The *m* value obtained in fitting the variant unfolding curve (0.61) is lower than the *m* value obtained in fitting the wild-type unfolding curve (0.69). To test whether this difference and apparent change in ΔG_u resulted from an inability to measure the CD signal from the fully

unfolded state, simulations were performed in which the data were extrapolated to plateau CD values at higher concentrations of guanidine; essentially identical estimates of ΔG_u and *m* were obtained. Nonetheless, due to the change in the *m* value, the two-state formalism (*38*) may overestimate thermodynamic decrements (*39*). Conservative lower bounds to $\Delta\Delta G_u$ are obtained by multiplying its C_{mid} value by the parent *m* value. Global fitting of the *allo*-Ile^{A2} variant unfolding transition using the native *m* value leads to large errors. Similar $C_{mid}-m$ compensation was observed in studies of *allo*-Ile^{A2} in the context of DKP-insulin (*15*). In studies of unrelated proteins, lower *m* values have sometimes been observed in association with a greater exposed hydrophobic surface in the absence of denaturant and/or existence of a native-state ensemble containing a distribution of incompletely folded forms of differing stability (*38*). The present crystallographic study, as well as previous NMR analysis of *allo*-Ile^{A2}-insulin, does not support such an interpretation here.

NMR Simulations. Simulated NOESY spectra were calculated using the program X-PLOR as described (*40*). The hydrogen atom positions were generated automatically by Insight II (Molecular Simulation Incorporation). To enable quantitative comparison, intramolecular ortho−meta NOE intensities of the aromatic ring of Tyr^{A14} were set at the same level. The rotational correlation time of insulin was assumed to be 2.5 ns. Order parameters for vectors between main-chain atoms were set at 0.85, between main chain and side chains at 0.80, and between side-chain atoms at 0.65.

Structural Comparisons. An estimate of the intrinsic variability among wild-type insulin crystal forms is provided by mean pairwise RMS deviations, defined as the average of RMSD values obtained in systematic pairwise alignment of main-chain atoms. This measure provides a baseline for the assessment of RMS deviations between the present structure and the native structures.

Chiral Nomenclature. The χ_1 dihedral angle of *allo*-Ile is ordinarily defined (as in Ile) by atoms N, C^α, C^β, and C^γ. The χ_2 dihedral angle of *allo*-Ile is likewise defined (as in Ile) by C^α, C^β, C^γ, and C^δ. Thus, Ile and *allo*-Ile side chains with similar χ_1 and χ_2 angles would exhibit aligned $-C_\gamma H_2-C_\delta H_3$ elements but displaced γ'-CH_3 moieties due to chiral inversion of the β-carbon. To our knowledge, only one high-resolution structure of a protein containing *allo*-isoleucine has been reported: a designed coiled−coil (PDB code 1RH4; ref *41*). In the reported structure, *allo*-isoleucine adopts dihedral angles of χ_1 171° (or −189°) and χ_2 176° (or −184°). In the present T-state protomer, *allo*-Ile^{A2} has a similar side-chain conformation as in the coiled−coil, whereas in the R-state its χ_1 value differs.

RESULTS

The receptor-binding activity of *allo*-Ile^{A2}-insulin is 50-fold lower than that of native insulin in accord with previous studies (*13*, *15*). CD studies demonstrate that the analogue exhibits native α-helix content (Figure 3A) and thermal stability (not shown). Studies of thermodynamic stability by guanidine denaturation indicate a rightward shift of the analogue's denaturation curve (Figure 3B). Under these conditions (see Materials and Methods), insulin is predominantly monomeric. An estimate of ΔG_u (3.2 ± 0.1 kcal/mol at 25 °C), as inferred from a two-state model, is nonetheless similar to that of native insulin (3.3 ± 0.1 kcal/mol) as the analogue's greater C_{mid} value is offset by a reduction in the *m* value (Table 1). We cannot exclude that *allo*-Ile^{A2}-insulin is slightly more stable than insulin. An upper bound (ΔG_u 3.6 kcal/mol) is obtained by the product of the analogue's C_{mid} value by the wild-type *m* value, suggesting that $\Delta\Delta G_u$, if nonzero, is less than 0.4 kcal/mol. In the apparent absence of a conformational change (see Materials and Methods), such *m* value effects are not well-understood.

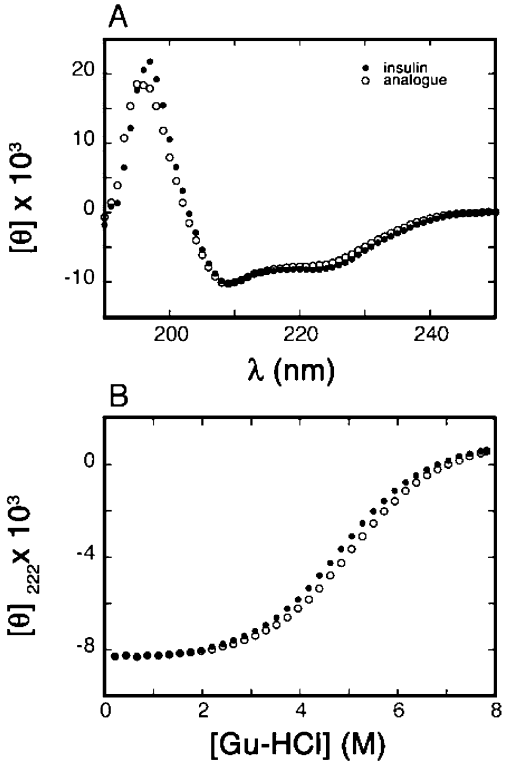

FIGURE 3: Comparative CD studies of *allo*-Ile^{A2}-insulin and native insulin. (A) Far-UV CD spectra of native insulin and chiral analogue exhibit similar features and inferred α-helix contents. (B) Guanidine denaturation studies as monitored by ellipticity at 222 nm. Although a rightward shift occurs in the unfolding transition, a compensating change in the *m* value is inferred, leading to similar estimates of ΔG_u (see Table 1).

Comparison of Crystal Structure to Native Insulin. The organization of the hexamer is essentially identical with that of native insulin in the same crystal form. No significant changes are observed in secondary structure, chain orientation, mode of assembly, or structure of Zn^{2+}-binding sites. We have chosen to use a native $T_3R^f_3$ structure (PDB code 1TRZ; ref *10*) as a standard because the unit cell dimensions, space group, and hexamer organization are similar to those of the present crystals.[5] Features of interest are then evaluated in relation to an extensive collection of native structures. This approach enables perturbations associated with the *allo*-Ile^{A2} substitution to be distinguished from the baseline structural variability of native insulin among crystal forms.[6]

Initial comparisons focused on alignment of the variant TR dimer and native TR dimer (PDB code 1TRZ) according

[5] Despite their similarities, the present crystals and those of 1TRZ (*10*) were grown under different conditions. In the latter, the $T_3R^f_3$-state was induced by high concentrations of chloride ion (0.75 M) in the absence of phenol. The potential phenol-binding pockets contain water molecules.

Table 3: Conformation of A2 Side Chains[a]

structure	lattice	protomer	(ϕ, ψ)	structure	lattice	protomer	(ϕ, ψ)
native $T_3R^f_3$	rhombohedral	T	−60.9, −34.0	native T_6	rhombohedral	T1	−55.2, −45.5
		R	−58.4, −35.5			T2	−53.6, −37.9
		T	−56.5, −37.6		monoclinic	⟨R⟩[b]	−59.6, −41.0
allo-Ile^{A2} $T_3R^f_3$	rhombohedral	R	−81.5, −21.8	native R_6	rhomobohedral	R1	−59.7, −37.2
						R2	−62.6, −39.1
KP-ins $T_3R^f_3$	rhombohedral	T	−68.6, −50.7	native T_2	cubic	T	−62.4, −30.9
		R	−92.0, −38.6				

[a] Native $T_3R^f_3$ structure is obtained from PDB code 1TRZ (*10*); KP-ins indicates analogue containing substitution Pro^{B28} → Lys and Lys^{B29} → Pro (*62*). Other PDB entries are native T_6, 4INS; native R_6, 1ZNJ and 1EV3; and native T_2, 1APH. [b] ⟨R⟩ represents the average of six R-state protomeric structures.

to their main-chain atoms. In this alignment, root-mean-square deviations (RMSD), excluding the A2 residue, are small. Values in the T-state are 0.45 Å (main chain) and 0.83 Å (side chain) and in the R-state, 0.54 Å (main chain) and 0.89 Å (side chain). Similar RMSD values are obtained in pairwise comparison with other crystal forms. Backbone conformations of residue A2 in the T- and R-states in this and other crystal structures are given in Table 3. Although differences are observed relative to the 1TRZ $T_3R^f_3$ hexamer, ϕ and ψ values of *allo*-Ile^{A2} remain in the α-helical region and are broadly consistent with values observed in other crystal forms. In accord with the analogue's unperturbed stability, packing of side chains in the core is similar (but not identical) to that of native insulin. The nonstandard A2 side chain is well-defined but differs in conformation between T- and R-state protomers as follows:

(i) T-State. Among native protomers, a charge-stabilized hydrogen bond or salt bridge is sometimes (but not always) observed between the side-chain carboxylate of Glu^{A4} and the α-amino group of A1. Accordingly, this distance ranges from 2.30 to 4.48 Å (PDB codes 4INS, 2INS, 1APH, 1BPH, 1CPH, 1DPH, 1BEN, 1MPJ, 1LPH, 1TRZ, 1TYL, 1TYM, 1G7A, and 3MTH). The corresponding distance for *allo*-Ile^{A2} insulin is 5.32 Å, which is significantly above the range of native values. Further, contact distances differing by more than 1.35 Å occur between respective A2 side chains (Ile^{A2} or *allo*-Ile^{A2}) and Leu^{A16}, Leu^{B11}, and Phe^{B25} as specified in Table 4. The main-chain (ϕ, ψ) conformation of *allo*-Ile^{A2} is (−56.5°, −37.6°), similar to that of Ile^{A2} in a native $T_3R^f_3$ hexamer (−60.9°, −34.0°; PDB code 1TRZ). The side-chain (χ_1, χ_2) conformation of *allo*-Ile^{A2} is (−142°, 179°) in the T-state, similar to that of Ile^{A2} in this native hexamer (−167°, 157°).

(ii) R-State. Among native R-state protomers, distances between 2.34 and 5.33 Å are observed between Glu^{A4} and the A1 α-amino group (PDB codes 1BEN, 1MPJ, 1LPH, 1TRZ, 1TYL, 1TYM, 1G7A, 3MTH, 1ZEG, 1ZEH, 1ZNJ, and 1EV6). The corresponding distance for *allo*-Ile^{A2} insulin is 8.10 Å, which (as in the T-state protomer) is significantly larger than native distances. Differences in core packing are also observed. Contact distances differing by more than 1.35 Å occur between respective A2 side chains and Leu^{A16}, Leu^{B11}, and Phe^{B25} (Table 4). The main-chain conformation (ϕ, ψ) of *allo*-Ile^{A2} is (−81.5°, −21.8°), which is similar to native values (−58.4°, −35.5° in the 1TRZ hexamer). The A2 side-chain conformation (χ_1, χ_2) is (62°, −173°). The χ_1 value is distinct from that observed in the native hexamer (−161°), whereas the χ_2 value is similar (−175°). The distinct χ_1 values of *allo*-Ile^{A2} lie outside of the observed range of Ile^{A2} in multiple $T_3R^f_3$ crystal forms (PDB codes 1BEN, 1MPJ, 3MTH, 1QJ0, 1ZNI 1TRZ, 1G7A, and 1G7B). This value ranges from 176 to 199°.

Table 4: Contacts of *Allo*-Ile^{A2} and Native Ile^{A2} Side Chains in Crystal Structures[a]

	T-state (Å)		R-state (Å)	
residues[b]	*allo*-Ile^{A2}	Ile^{A2}	*allo*-Ile^{A2}	Ile^{A2}
A2-$C_{\delta1}$−A16-$C_{\delta2}$	6.75	4.40	6.41	3.96
A2-$C_{\delta1}$−A19-C_{γ}	4.37	3.45	3.90	4.04
A2-$C_{\delta1}$−B11−$C_{\delta1}$	5.36	3.99	6.19	4.71
A2-$C_{\delta1}$−B15−$C_{\delta1}$	3.74	3.58	4.36	3.27
A2-$C_{\delta1}$−B25−$C_{\delta1}$[c]	5.42	7.32	10.25	11.9
A2-$C_{\delta1}$−B26−$C_{\delta1}$	3.65	5.00	5.26	5.33

[a] Native $T_3R^f_3$ structure is obtained from PDB code 1TRZ (*10*). [b] Both *allo*-Ile^{A2} and native Ile^{A2} pack in the core against the side chains of Leu^{A16}, Tyr^{A19}, Leu^{B11}, Leu^{B15}, and Tyr^{B26}. [c] In the T- and R-states, Phe^{B25} exhibits two distinct conformations at the dimer interface.

Packing elsewhere in T- and R-state cores is similar to that observed in a collection of wild-type crystal structures (Figure 4). In essence, differences in packing relative to native insulin reflect simple inversion of A2 chirality in the R-state and an altered conformation of the *allo* side chain in the T-state. Differences in packing extend to the C-terminal B-chain β-strand. As observed among native hexamers, the T-state of *allo*-Ile^{A2}-insulin exhibits a shorter distance between the amide NH of Phe^{B25} and the carbonyl oxygen of Tyr^{A19} (N···O distance, 3.39 Å) than is observed in the R-state (N···O distance, 4.73 Å). Corresponding distances in native crystal structures are 2.79−3.40 Å (T-states; PDB codes 4INS, 2INS, 6INS, 1APH, 1BPH, 1CPH, 1DPH, 1BEN, 1MPJ, 1TRZ, 1TYL, 1TYM, 1LPH, and 3MTH) and 4.10−4.88 Å (R-states; PDB codes 1BEN, 1MPJ, 1TRZ, 1TYL, 1TYM, 1LPH, 3MTH, 1G7A, 1ZEG, 1ZEH, and 1ZNJ). Thus, B25-A19 distances in the *allo*-Ile^{A2} hexamer are at or near the upper end of values previously observed in T- and R-states; neither is consistent with the formation of a hydrogen bond.

Ligand-Binding Sites. The hexamer contains three symmetry-related phenolic ligands. Their environment and packing interactions are well-determined and in accord with previous crystal structures (*24*). Phenol molecules are bound in elliptically shaped binding sites located on the interfaces

[6] Hydrophobic-core packing schemes in a collection of wild-type crystal structures (PDB codes 1APH, 1BPH, 1CPH, 1DPH, 1G7A, 1LPH, 1PID, 1TRZ, 1TYL, 1TYM, 1ZNI, 2INS, and 4INS) are generally similar but also exhibit structural variability. For example, the χ_1 and χ_2 dihedral angles of Leu^{B15} in the T-state of 1LPH and 1PID T-state protomers differ from their values in the majority of crystal forms. Analogous variation in Leu^{B15} χ_2 occurs in the R-state of 1LPH.

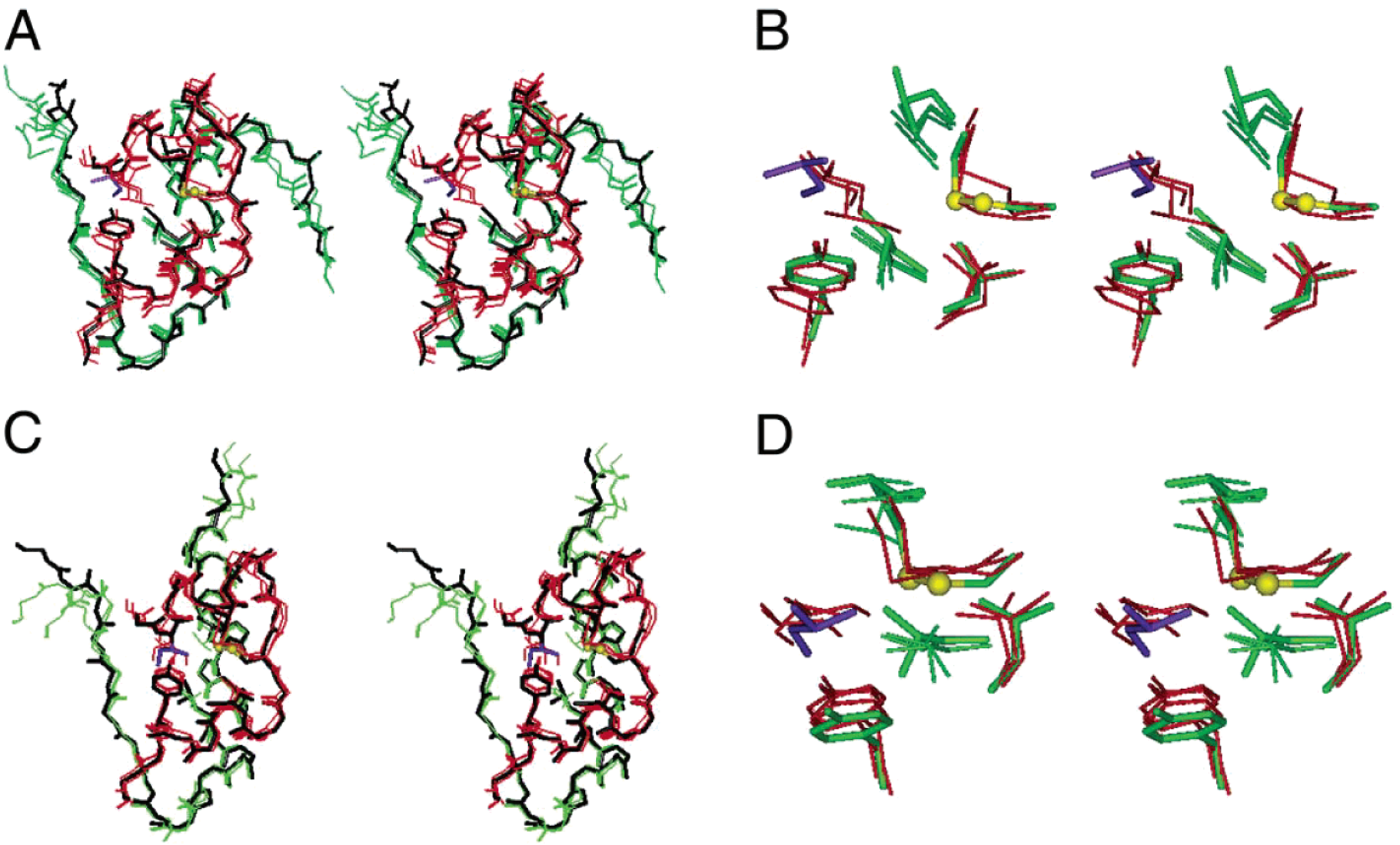

FIGURE 4: Stereoview of crystal structure of *allo*-Ile^{A2}-insulin in relation to crystal structures of insulin. (A) T-state protomer of *allo*-Ile^{A2}-insulin (black) and crystal structures of insulin (PDB codes 4INS and 1TRZ). A-chains of native insulin are shown in red and B-chains in green. The *allo*-Ile^{A2} side chain is shown in purple and cystine A6-A11 in yellow. Structures are aligned with respect to main-chain atoms of residues A2-A20 and B9-B19. (B) Stereoview of packing schemes in the T-state hydrophobic core. Environment of *allo*-Ile^{A2} in relation to cystine A6-A11, Leu^{A16}, Tyr^{A19}, Leu^{B11}, and Leu^{B15}. Side chains of the chiral analogue are shown as thick sticks, whereas these of native insulin are thin lines. Side chains in the analogue are green, purple (*allo*-Ile^{A2}), or yellow (cystine A6-A11). Side chains in native structures are red (A-chain) or green (B-chain). (C) R-state protomer of *allo*-Ile^{A2}-insulin and crystal structures of insulin (black) and insulin analogues (PDB codes 1TRZ, 1LPH, and 1G7A). Coloring scheme is as in panel A. Structures are aligned with respect to main-chain atoms of residues A2-A20 and B3-B28. (D) Stereoview of packing schemes in the R-state hydrophobic core. Coloring scheme is as in panel B.

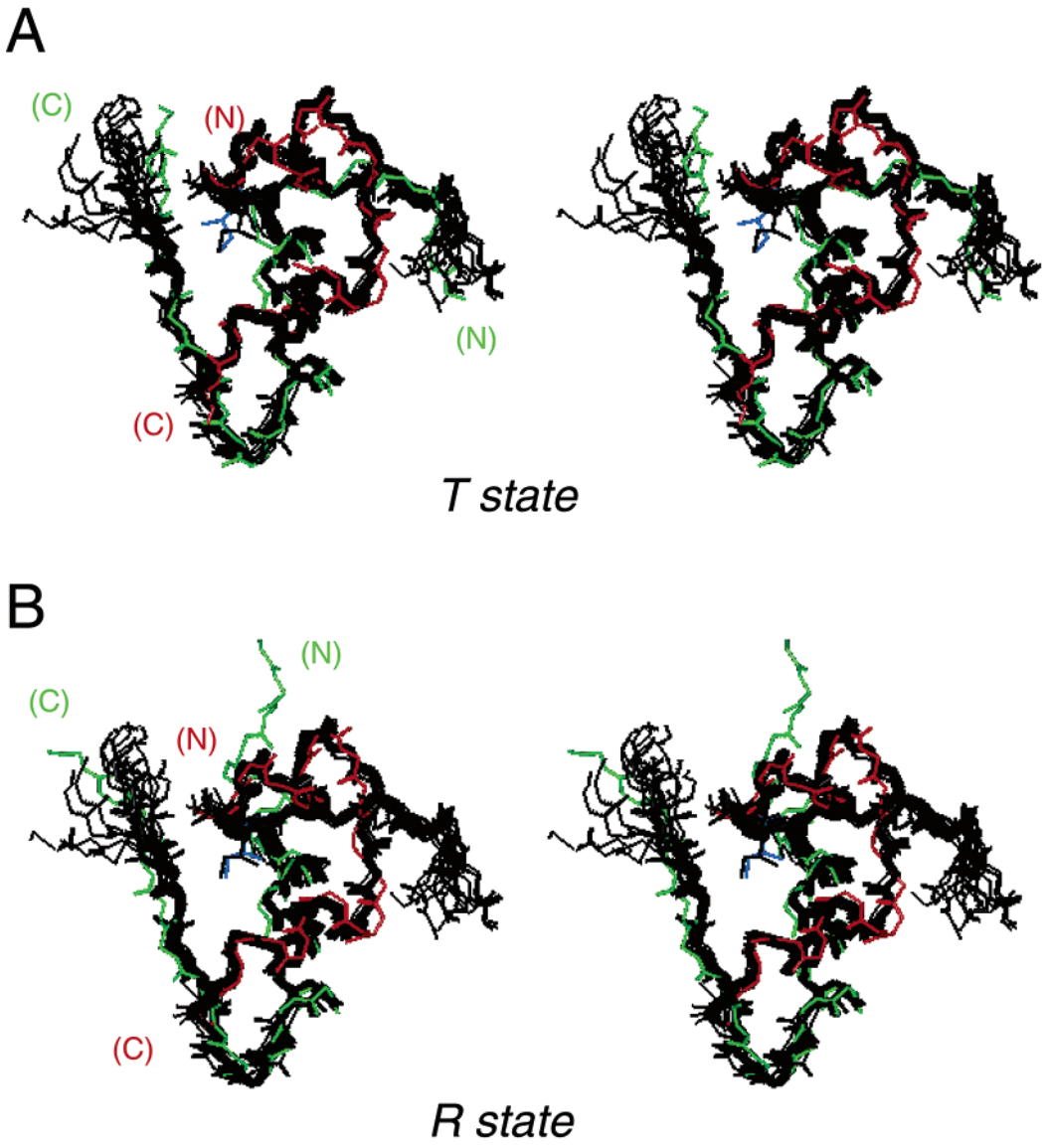

FIGURE 5: Crystal structure of *allo*-Ile^{A2} insulin (red and green) and solution structure of *allo*-Ile^{A2}-DKP-insulin (black) in the (A) T-state and (B) R-state. DG/RMD ensemble is as described (ref *15*; PDB code 1KMF). The A-chain of the crystal structure is shown in red and the B-chain in green. Structures in panel A are aligned with respect to main-chain atoms of residues A1-A21 and B3-B28; structures in panel B are aligned with respect to the main chain of residues A1-A21 and B9-B28.

between R^f monomers. The orientation of the phenol is stabilized in part by hydrogen bonds from the phenolic hydroxyl group to the carboxyl oxygen of Cys^{A6} (O···O distance, 2.77 Å) and the nitrogen of Cys^{A11} (O···N distance, 2.81 Å) (Supporting Information). The pocket is lined by the residues A6, A10, A11, and A16; residues B7, B10, B11, and B14; and in an adjoining R-state protomer B5, B6, and B9. This binding mode is characteristic of all insulin−phenol complexes (*24*, *42*−*44*).

Small differences among crystal structures are often observed in the detailed orientation of the phenol and conformation of neighboring side chains (Supporting Information). Upon alignment of the main-chain atoms of the present hexamer with those of phenol- and methylparaben ligands in $T_3R^f_3$ hexamers (PDB codes 1MPJ, 1LPH, and 3MTH), the position of the present phenolic ligand exhibits an average pairwise RMSD of 0.57 Å relative to its position in the hexamers described previously. This is within the range of variation among the phenol- and methylparaben ligands among native $T_3R^f_3$ structures, as their main pairwise alignment yields a similar phenol-specific RMSD of 0.49 Å. In the Supporting Information, the position of the bound phenol in the *allo*-Ile^{A2} hexamer is shown relative to the range of its positions in native hexamers. The mean thermal *B* factor of the phenolic ligand (38.0 ± 1.7 Å^2) is in the upper range of *B* factors observed among main-chain atoms (27.2 ± 8.7 Å^2 in the T-state and 28.8 ± 10.5 Å^2 in the R-state) and side chains (29.4 ± 10.3 and 29.1 ± 11.9 Å^2 in the T- and R-states, respectively) but similar to the *B* values of water molecules (33.83 ± 12.2 Å^2). As previously noted among native structures (*45*), the phenol-binding site in the $T_3R^f_3$ hexamer of *allo*-Ile^{A2}-insulin is similar to a pocket in 4-Zn ($T_3R^f_3$) insulin formed in the absence of phenolic ligands. In the absence of phenol, this pocket is filled by water and in some cases ions such as Zn^{2+} or chloride (*6*, *10*, *45*, *46*).

The environment of the Zn^{2+} ions is also well-determined and in accord with previous structures of $T_3R_3^f$ hexamers.

As described previously in relation to the phenol-binding pocket, the alignment of main-chain atoms between the present and the previous phenol- and methylparaben liganded $T_3R^f_3$ hexamers (PDB codes 1MPJ, 1LPH, and 3MTH) demonstrates little change in the position of axial Zn^{2+} ions. RMSD values are 0.36 Å (the average for a T_3 trimer site) and 0.25 Å (the average for an R^f_3 trimer site) relative to corresponding baseline RMSD values of 0.34 and 0.33 Å among previous structures. Such structures exhibit distances between the zinc ion and the $N^{\epsilon 2}$ of His^{B10} residues within the range of 1.76−2.16 Å; a bond distance of 2.10 Å is typical for octahedral geometry, whereas a distance of 2.00 Å is typical for tetrahedral geometry (PDB codes 4INS, 2INS, 1BEN, 1TRZ, 1TYL, 1TYM, 1MPJ, 1LPH, 1G7A, 1EV3, 1ZNJ, and 1EV6). In accord with these trends, corresponding distances in the T- and R-state trimers of *allo*-Ile^{A2}-insulin are 1.99 and 2.08 Å, respectively. The electron density of zinc ligands are shown in the Supporting Information. In the high-resolution structure of two $T_3R_3^f$ insulin hexamers (using crystals containing a doubled C-axis dimension grown in zero gravity and observed at 100 K to a resolution of 1.2 and 1.3 Å), three of the four axial zinc ions are tetrahedrally coordinated; the fourth is statistically disordered with both tetrahedral and octahedral coordination (*46*). In the present structure at lower resolution, we see no evidence of statistical disorder in either Zn-binding site. Possible electron density in the neighborhood of the Zn ions corresponding to a fourth ligand was not well-defined, and so potential ligands were not included in the model. The absence of such density stands in contrast to the well-defined conformations of side chains (such as Lys^{B29}) that can be poorly ordered in some wild-type structures (Supporting Information).

Comparison of Crystal Structure and Solution Ensemble. The crystal structure of *allo*-Ile^{A2}-insulin exhibits similarities and differences in relation to NMR-derived models of *allo*-Ile^{A2}-DKP-insulin (Figure 5). The crystallographic hexamer contains both T- and R-state protomers, whereas only a T-like secondary structure is observed in solution (*15*). The overall structure of the crystallographic T-state protomer (and R-state protomer exclusive of residues B1-B8) of *allo*-Ile^{A2}-insulin resembles the NMR models. Surprisingly, however, local packing of *allo*-Ile^{A2} in NMR models more closely resembles that of the R-state protomer. Key diagnostic distances from *allo*-Ile^{A2} in the T- and R-state protomers are given in Table 5 in relation to observed NOEs. At least six *allo*-Ile^{A2} interresidue NOE contacts (shown in bold) are in accord with distances in the crystallographic R-state protomer but not the T-state protomer.[7] RMSDs of *allo*-Ile^{A2}-insulin in relation to NMR models of *allo*-Ile^{A2}-DKP-insulin are somewhat larger than deviations observed among native T- or R-state crystal structures (Supporting Information). This may, in part, reflect encagement of the analogue within a hexamer. Evidence that such encagement damps conformational fluctuations in native insulin has recently been described (*47*). A similar pattern of RMSDs is observed on alignment of the NMR structure of DKP-insulin (ref *4*; PDB code 1LNP) with crystallographic protomers of native insulin. The mean distance between the NH of Phe^{B25} and the carbonyl oxygen of Tyr^{A19} in the solution ensemble (N···O distance, 3.61 ± 0.6; corresponding to the average and standard deviation among 15 NMR models) is similar to the T-state value; the range of values extends to 4.8 Å and thus encompasses distances sometimes observed in native R-states (see previously). It is not clear whether the distribution of distances in the NMR-derived ensemble is physical or a consequence of informational uncertainty.

Table 5: Comparison of Observed and Predicted NOEs Involving *Allo*-Ile^{A2}

A2 proton[a]	contact	NOE intensity[b]	distance in crystal[c]	
			T-state	R-state
H_α	*allo*-Ile^{A2} $H_{\gamma 1,2}$	m	2.11	3.35
H_α	Val^{A3} H_N	w	3.52	3.42
H_α	Gln^{A5} H_β	m	3.22	3.62
H_β	*allo*-Ile^{A2} $H_{\delta 1}$	s	2.53	2.45
H_β	**Val^{A3} H_N**	**w**	**2.67**	**4.13**
H_β	**Tyr^{A19} $H_{\delta 1,2}$**	**m**	**>5.00**	**3.36**
H_β	**Tyr^{A19} $H_{\epsilon 1,2}$**	**m**	**>5.00**	**3.08**
H_N	*allo*-Ile^{A2} H_β	m	3.04	2.60
H_N	*allo*-Ile^{A2} $H_{\gamma 1,2}$	s	3.63	1.77
H_N	*allo*-Ile^{A2} $H_{\gamma'}$	w	1.64	3.75
H_N	*allo*-Ile^{A2} $H_{\delta 1}$	m	4.24	3.41
$H_{\gamma 1,2}$	Tyr^{B26} H_α	w	4.67	>5.00
$H_{\gamma 1,2}$	Tyr^{B26} $H_{\delta 1,2}$	w	3.99	4.28
$H_{\gamma 1,2}$	Thr^{B27} H_α	w	>5.00	>5.00
$H_{\delta 1}$	Val^{A3} H_α	w	>5.00	>5.00
$H_{\delta 1}$	Val^{A3} H_N	m	4.78	4.25
$H_{\delta 1}$	Tyr^{A19} $H_{\delta 1,2}$	s	3.38	2.72
$H_{\delta 1}$	Tyr^{A19} $H_{\epsilon 1,2}$	s	4.27	3.80
$H_{\delta 1}$	**Tyr^{B26} H_α**	**m**	**2.51**	**3.62**
$H_{\delta 1}$	**Tyr^{B26} $H_{\delta 1,2}$**	**w**	**2.18**	**3.25**
$H_{\delta 1}$	**Tyr^{B26} $H_{\epsilon 1,2}$**	**w**	**2.74**	**4.11**
$H_{\delta 1}$	Thr^{B27} H_α	w	4.93	>5.00
$H_{\gamma'}$	Tyr^{A19} $H_{\delta 1,2}$	s	3.17	3.28
$H_{\gamma'}$	Tyr^{A19} $H_{\epsilon 1,2}$	s	2.73	3.36

[a] $H_{\gamma 1}$ and $H_{\gamma 2}$ are unresolved. [b] NOEs are classified as strong (s), medium (m), or weak (w) as follows: s ≤ 2.7 Å; 2.7 Å < m ≤ 3.4 Å; and 3.4 Å < w ≤ 5.0 Å. [c] Distance is calculated as average distance ($1/R_{av}^6 = \mathring{a}_i 1/R_i^6$) wherever multiple protons are involved. NOEs in *allo*-Ile^{A2}-DKP-insulin more consistent with the R- than the T-state are highlighted in bold. Calculations are based upon the representative native $T_3R^f_3$ hexamer 1TRZ (*10*).

General similarities are observed in solution and in the crystal regarding how *allo*-Ile^{A2} packs within the hydrophobic core. Although subtle structural variations are observed (Figure 6), the degree of variation is similar to that seen among different crystal structures of native insulin itself (Supporting Information). χ_1 and χ_2 dihedral angles of *allo*-Ile^{A2} in the R-state protomer (62 and −173°, respectively) are similar to those in *allo*-Ile^{A2}-DKP-insulin in solution (58 ± 4 and −172 ± 9°). In the crystallographic T-state, the χ_1 angle of *allo*-Ile^{A2} (−137°) differs from the mean χ_1 value of *allo*-Ile^{A2} in solution, whereas its χ_2 angle (−181°) is similar. By contrast, the conformation of Ile^{A2} observed in the parent monomer DKP-insulin in solution (*4*) resembles that observed in the crystallographic T-state of native insulin. Calculated solvent accessibilities of the nonstandard A2 side chains are in each case negligible, as expected given the packing of Ile^{A2} in the native core.

[7] The crystal structure of *allo*-Ile^{A2}-insulin is in overall accord with interresidue NOEs in the spectrum of *allo*-Ile^{A2}-DKP-insulin. Significant differences were found only in (a) the B1-B7 segment of the R-state as expected; (b) NOEs involving mobile side chains on the protein surface (i.e., Thr^{A8} γ-CH_3); and (c) NOEs involving side chains that have variable conformations among different crystal forms of native insulin. No significant backbone distance violations are observed (see Table 5 for observed and predicted NOEs involving *allo*-Ile^{A2}).

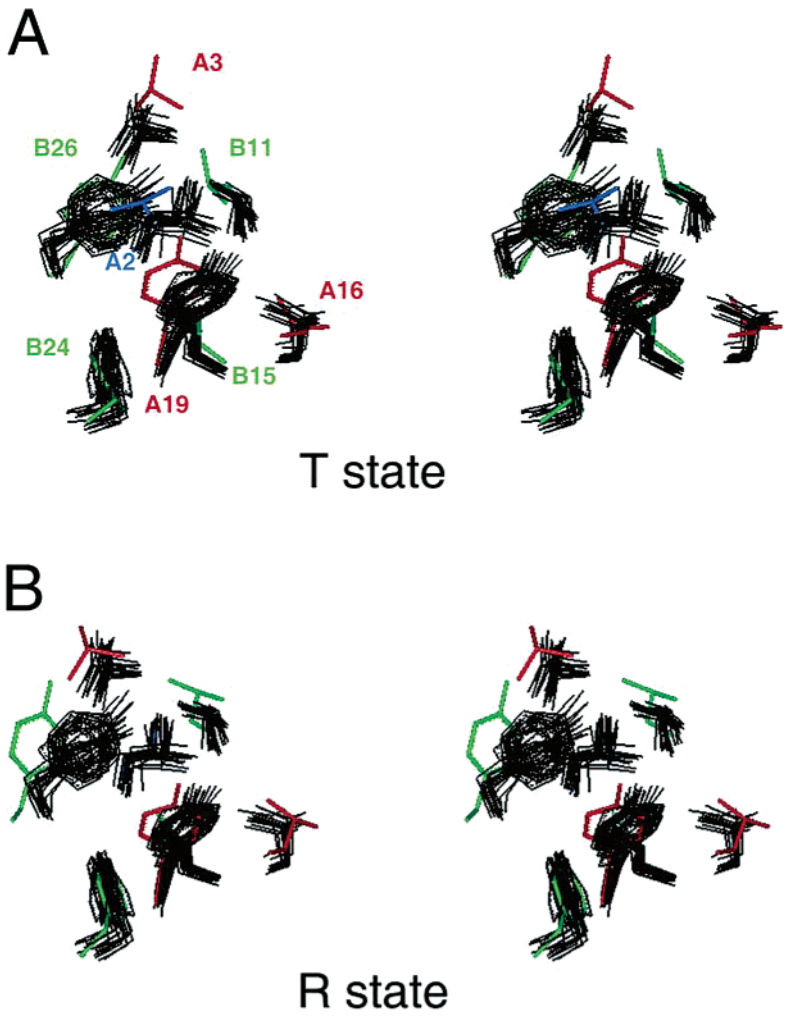

FIGURE 6: Comparison of packing schemes in the hydrophobic core in crystal and in solution. (A) Environment of *allo*-Ile^{A2} (blue) and neighboring side chains in the T-state crystallographic protomer in relation to Val^{A3}, Leu^{A16}, Tyr^{A19} (red), Leu^{B11}, Leu^{B15}, Phe^{B24}, and Tyr^{B26} (green) in an ensemble solution structure of *allo*-Ile^{A2}-DKP-insulin (black; PDB code 1KMF). (B) Corresponding environment of *allo*-Ile^{A2} (blue) and neighboring side chains in the R-state protomer in relation to the solution ensemble.

DISCUSSION

Structure−function relationships in insulin have been extensively investigated by mutagenesis and chemical modification (*9*, *13*). Structures of selected analogues have been determined by X-ray crystallography or NMR spectroscopy. Crystal structures are in general more precise than NMR models, and their accuracy is more readily evaluated by cross-validation. NMR studies of insulin have been facilitated by protein engineering (*3*, *4*, *16*), which circumvents the native protein's complex self-association properties at neutral pH. We have recently described NMR studies of Ala^{A2} and *allo*-Ile^{A2} analogues in the context of the engineered DKP monomer (*15*, *28*). The resulting distance geometry (DG) ensembles exhibit varying degrees of precision, reflecting in part physical disorder and informational uncertainty; the extent to which the variant structures were influenced by structural interactions between the A2 substitution and the DKP B-chain template could not be evaluated. To our knowledge, the present study represents the first comparative study of the same amino acid substitution by both NMR and crystallographic methods. An independent crystal structure of *allo*-Ile^{A2} was motivated by the biological importance of this analogue in relation to models of receptor binding (see next).

Insulin Structure and Assembly. Insulin provides a biophysical model for analysis of the affects of protein assembly on the structure and dynamics of a protein (*47*−*49*). Simulated NOESY spectra (*40*) derived from crystallographic protomers and NMR models (Figure 7A−C) are thus of interest in relation to observed spectra (Figure 7D). The region shown contains NOEs between aromatic protons (Figure 7, vertical axis) and aliphatic protons (Figure 7, horizontal axis). T-state features are highlighted in red in Figure 7 and R-state features in green. In solution, certain T-state-specific NOE features (i.e., cross-peaks *a*, *b*, and *d* in Figure 7A) are prominent (Figure 7A,D). These NOEs are inconsistent with the R-state simulation (Figure 7B). The observed NOESY spectrum nevertheless displays more similarities to simulated spectra of the R-state crystallographic protomer (excepting residues B1-B8; Figure 7B) than to the spectrum calculated on the basis of the crystallographic T-state (Figure 7A). For example, strong NOE contacts between Tyr^{A19} H_δ and *allo*-Ile^{A2} $H_{\delta 1}$ (*h* in Figure 7C), prominent in the observed spectra (Figure 7D), are recapitulated by the simulated R-state (but not T-state) NOESY spectrum. Similarly, the observed spectrum exhibits such R-state specific features as contacts between Phe^{B24} and Leu^{B15} (cross-peaks *i* and *j* in Figure 7B). The absence of

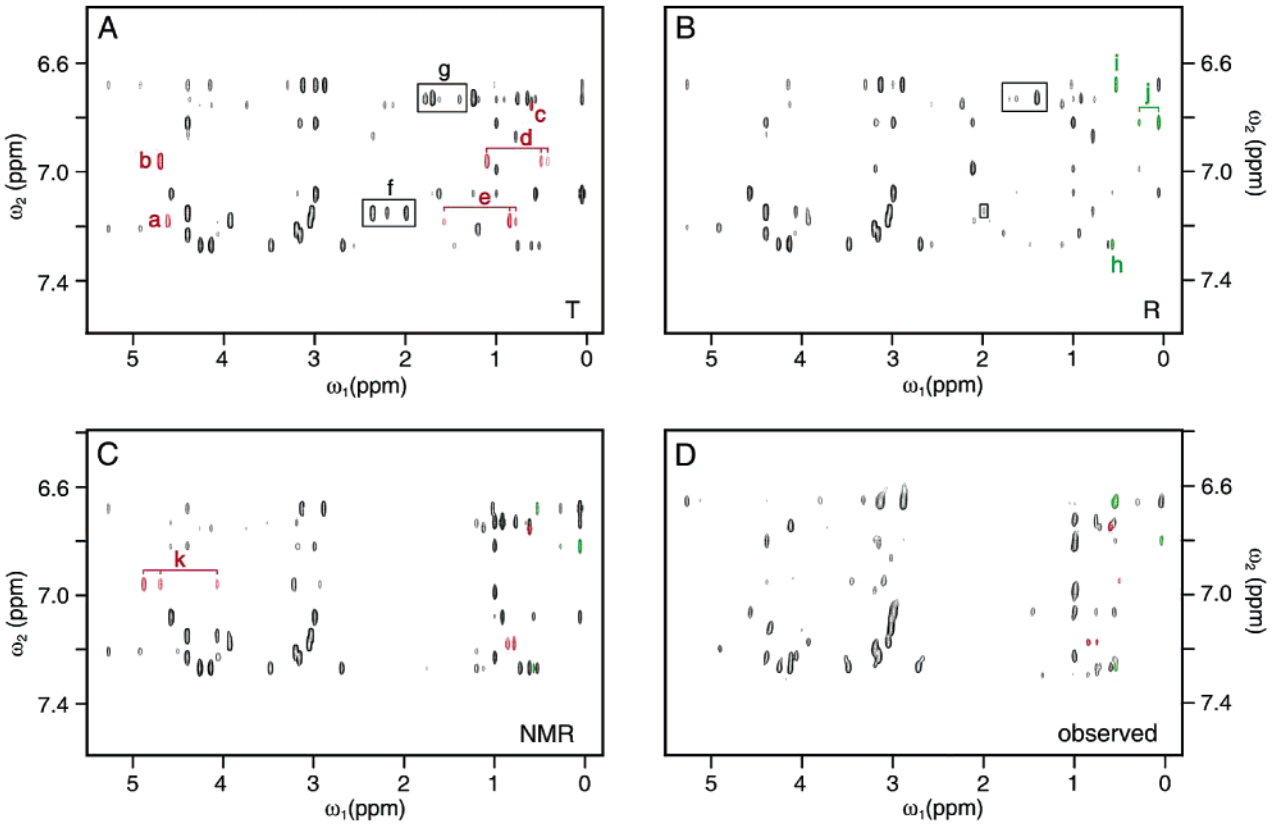

FIGURE 7: Comparison of experimental and simulated NOESY ^{1}H NMR spectra of *allo*-Ile^{A2} analogues. (A−C) Simulated spectra back-calculated from the crystallographic T-state protomer (A), R-state protomer (B), or NMR-derived DG/RMD ensemble of *allo*-Ile^{A2}-DKP-insulin (C; ref *15*). (D) Corresponding region of the experimental NOESY spectrum *allo*-Ile^{A2}-DKP-insulin. T-state-specific NOEs are shown in red; R-state-specific NOEs are shown in green. Simulated and experimental data were normalized with respect to the ortho−meta cross-peak of Tyr^{A14}; similar contour levels are shown in panels A−D, reflecting an experimentally obtained signal-to-noise ratio. A uniform rotational time of 2.5 ns was assumed. Simulated and experimental mixing times were, in each case, 200 ms. The experimental temperature was 37 °C, and the protein concentration was 1.2 mM. Boxes indicate NOE contacts involving a flexible side chain (Glu^{A17} $H_{\beta,\gamma1,\gamma2}$, Lys^{B28} $H_{\beta,\gamma,\delta}$) that are predicted in T- and R-state simulations but not observed. Selected NOEs are labeled as follows: (a) Phe^{B1} H_δ−Ser^{A12} H_α; (b) His^{B5} H_δ−Ser^{A9} H_α; (c) Tyr^{A19}H_ϵ−*allo*-Ile^{A2}H_γ; (d) His^{B5} H_δ−Ile^{A10} $H_{\gamma1,2}$ and His^{B5} H_δ−Ile^{A10} H_δ; (e) Phe^{B1} H_δ−Leu^{A13} H_β and Phe^{B1} H_δ−Leu^{A13} $H_{\delta1,2}$; (f) Tyr^{A14} H_δ−Glu^{A17} $H_{\beta2}$ and Tyr^{A14} H_δ−$H_{\gamma1,2}$; (g) Tyr^{B26}H_ϵ−Lys^{B28}$H_{\beta1,2}$, Tyr^{B26}H_ϵ−Lys^{B28}H_γ, and Tyr^{B26}H_ϵ−Lys^{B28}H_δ; (h) Tyr^{A19} H_δ−*allo*-Ile^{A2} H_δ; (i) Phe^{B24} H_δ−Leu^{B15} $H_{\delta2}$; (j) Phe^{B24} H_ϵ−Leu^{B15} $H_{\beta2}$ and Phe^{B24} H_ϵ−Leu^{B15} $H_{\delta1}$; and (k) His^{B5} H_δ−Cys^{A7} H_α, His^{B5} H_δ−Ser^{A9} H_α, and His^{B5} H_δ−Thr^{A8} H_α.

these features in the spectrum predicted by the crystallographic T-state protomer reflects its altered pattern of core packing. These observations indicate that some R-state-specific features of core packing can be uncoupled from the transition in secondary structure involving B1-B8. NOE contacts involving a flexible side chain (cross-peaks *f* and *g* in Figure 7A) are predicted in T- or R-state simulations (boxes in Figure 7A,B) but not observed in solution (Figure 7D). Their attenuation in solution presumably reflects flexibility in the solvated surface of the monomer. In this respect, observed spectra are in accord with the average of simulated spectra calculated for each member of the DG/restrained molecular dynamics (RMD) ensemble (Figure 7C). Similarity between the observed spectrum and the average DG/simulated annealing (SA) spectrum is in accord with the absence of significant restraint violations in the ensemble (*15*). Differences are likely to reflect local variation in side-chain mobility, which would modulate NOE intensities but is not included in the simulations.

Implications for Receptor Binding. How does insulin bind to the insulin receptor? Paradoxical analogues *allo*-Ile^{A2}-insulin and mini-proinsulin (*50*), although of low activity, each exhibit nativelike protein surfaces. In particular, the classical receptor-binding surface of *allo*-Ile^{A2}-insulin is similar to that of native insulin (*9*, *25*, *30*). In light of the low activity of *allo*-Ile^{A2}-insulin, this finding seems analogous to the observation of native structure in mini-proinsulin (*14*). Such a lack of correlation between structure and function is in accord with the hypothesis that insulin undergoes a change in conformation upon receptor binding (*2*, *9*, *14*). Whereas the tether between chains in mini-proinsulin presumably hinders reorganization on receptor binding, we suggest that the low activity of *allo*-Ile^{A2}-insulin reflects steric incompatibility between the nonstandard side chain and a chiral pocket in the insulin receptor. This pocket, predicted to play a central role in hormone−receptor recognition, is not considered or identified in an atomic model of the insulin−insulin receptor complex proposed by C. Yip and colleagues based upon electron-microscopic image reconstruction (*31*, *51*). The EM-derived model contains a docked T-state insulin protomer and so excludes possible effects of induced fit on hormone−receptor recognition.

A structural model for exposure of Ile^{A2} on receptor binding is provided by the truncated analogue DPI. When amidated at B25, DPI exhibits native potency (*20*, *21*). Crystal structures of DPI (*7*, *8*, *19*), *des*-hexapeptide (B24-B30) (*52*), and *des*-heptapeptide (B25-B30; ref *11*) demon-

strate overall maintenance of the protein's α-helical core, flexibility of the B1-B9 segment, and increased exposure of selected A-chain side chains, including Ile^{A2} and Val^{A3}. Analogous exposure of these A-chain residues may underlie the anomalous increase in activity observed on substitution of the Phe^{B24} anchor by D-amino acids (*9*, *17*, *18*). D-substitutions at B12, B25, and A8—side chains in native insulin proposed to contact the receptor—by contrast cause severe decrements in activity (*53*−*55*). On this basis, Phe^{B24} is proposed to define a site of conformational change on receptor binding (*2*, *9*). Chiral mutagenesis of this and other possible hinge sites promises to provide a general approach by which to unmask hidden structure−activity relationships. To our knowledge, structures of high-potency analogues containing D-amino acids at B24 have not been determined and would be of future interest. Their biological potencies seem at odds with the EM-derived model of the hormone−receptor interface (*31*, *51*).

Dual Role of Ile^{A2} in Structure and Function. Inspection of the sequences of 80 members of the vertebrate insulin family reveals a cluster of conserved core residues, including Ile^{A2}, Leu^{A16}, Tyr^{A19}, Leu^{B11}, and Leu^{B15} (*56*). Our results highlight different roles for Ile^{A2} and Leu^{A16}. Although each packs in the hydrophobic core, only Ile^{A2} is proposed to contact the insulin receptor. By contrast, substitutions at A16 perturb structure and stability but (unlike A2 analogues) retain substantial binding activity (*57*). Studies of peptide models of proinsulin folding intermediates suggest that Leu^{A16} participates—together with cystine B19-A20 and the central α-helix of the B-chain—in a specific folding nucleus (*58*). Like Leu^{A16}, the side chain of Ile^{A2} also plays a structural role: anchoring the A1-A8 recognition α-helix (*28*). A1-A8 is peripheral to the specific folding nucleus, however, and so mutations in this region permit native disulfide pairing (*4*, *58*). Co-evolution of insulin and the insulin receptor have apparently led to stabilization of a recognition α-helix by β-branched residues (Ile^{A2}, Val^{A3}) of low intrinsic helical propensity.

The proposed receptor-binding surfaces of insulin include Gly^{A1}, Ile^{A2}, Val^{A3}, Tyr^{A19}, Asn^{A21}, Val^{B12}, Tyr^{B16}, Gly^{B23}, Phe^{B24}, and Phe^{B25} (*9*, *25*, *30*, *59*). Detachment of the B-chain β-strand on receptor binding would expose Ile^{A2} and Val^{A3} as part of a hidden surface (*2*, *14*). This model may underestimate the extent of induced fit in the B-chain. An example is provided by the T → R transition (as observed here and in classical crystal structures of insulin hexamers; refs *6* and *24*). Change in the secondary structure of the B1-B8 segment is accompanied by changes in the dihedral angles of cystine A7-B7 and in the Ramanchandran conformation of Gly^{B8}. Following such a transition, the invariant side chain of Leu^{B6}—a core T-state residue implicated by mutagenesis in receptor binding (*60*)—would be exposed. Conversely, the environment of cystine A7-B7 changes from exposed and solvated (T-state) to partially buried within a nonpolar crevice (R-state). The T → R transition thus alters the topology and polarity of insulin's surface. Assessment of its relevance to receptor recognition will require high-resolution structures of a hormone−receptor complex.

Residues outside the classical binding site of insulin may also contact the receptor. Analogues with substitutions at A13 or B17, for example, exhibit anomalous binding and biological properties (*61*). A second receptor binding site spanning these residues has been proposed to rationalize otherwise puzzling aspects of receptor binding, including the existence of complexes of different stoichiometry, affinity, kinetic lifetimes, and negative cooperativity (*61*). The existence of two binding sites—a classical site that overlaps the dimer interface and a second site involving hexamer-forming residues—would allow a single insulin molecule to interpose between the two α subunits within the $\alpha_2\beta_2$-holoreceptor (*61*). It would be of future interest to test this model in relation to mechanisms of transmembrane signaling. We imagine that engulfment of the hormone between α-subunits of the holoreceptor would provide a hydrophobic milieu conducive to structural reorganization. The paradoxical structure and function of *allo*-Ile^{A2}-insulin suggest that Ile^{A2} functions as a core side chain unmasked in the complex to pack at a novel hormone−receptor interface.

ACKNOWLEDGMENT

We thank W. Jia for circular dichroism measurements and data processing; Q. X. Hua for assistance with NOESY simulations; S. Nakagawa for receptor-binding measurements in the Diabetes Research and Training Center of the University of Chicago; a reviewer for guidance regarding crystallographic methods and comparison with prior insulin structures; and G. G. Dodson and D. F. Steiner for helpful discussion. This is a contribution from the Cleveland Center for Structural Biology.

SUPPORTING INFORMATION AVAILABLE

Six figures showing ribbon models of T- and R-states of *allo*-Ile^{A2}-insulin; relationship of structure to prior crystal structures of insulin; space-filling representation of native R-state protomer; electron density of a phenol molecule bound in the R^f_3 trimer of $T_3R^f_3$ insulin; electron density of zinc ligands and the Lys^{B29} side chain; and an alignment of *allo*-Ile^{A2}-insulin with previous crystals of phenol−insulin complexes. Two tables providing RMSD values for comparison between the present structure and the prior crystal structures of native insulin or NMR structure of *allo*-Ile^{A2}-DKP-insulin. This material is available free of charge via the Internet at http://pubs.acs.org.

NOTE ADDED AFTER ASAP

Figure 5 was incorrect in the version published on the Web 10/16/03. The correct version of the paper was published 10/24/03.

REFERENCES

1. Dodson, G., and Steiner, D. (1998) The role of assembly in insulin's biosynthesis, *Curr. Opin. Struct. Biol. 8*, 189−194.
2. Hua, Q. X., Shoelson, S. E., Kochoyan, M., and Weiss, M. A. (1991) Receptor binding redefined by a structural switch in a mutant human insulin, *Nature 354*, 238−241.
3. Olsen, H. B., Ludvigsen, S., and Kaarsholm, N. C. (1996) Solution structure of an engineered insulin monomer at neutral pH, *Biochemistry 35*, 8836−8845.
4. Hua, Q. X., Hu, S. Q., Frank, B. H., Jia, W., Chu, Y. C., Wang, S. H., Burke, G. T., Katsoyannis, P. G., and Weiss, M. A. (1996) Mapping the functional surface of insulin by design: structure and function of a novel A-chain analogue, *J. Mol. Biol. 264*, 390−403.
5. Blundell, T. L., Cutfield, J. F., Cutfield, S. M., Dodson, E. J., Dodson, G. G., Hodgkin, D. C., Mercola, D. A., and Vijayan, M.

(1971) Atomic positions in rhombohedral 2-zinc insulin crystals, *Nature 231*, 506−511.
6. Bentley, G., Dodson, E., Dodson, G., Hodgkin, D., and Mercola, D. (1976) Structure of insulin in 4-zinc insulin, *Nature 261*, 166−168.
7. Bi, R. C., Dauter, Z., Dodson, E., Dodson, G., Giordano, F., and Reynolds, C. (1984) Insulin structure as a modified and monomeric molecule, *Biopolymers 23*, 391−395.
8. Dai, J.-B., Lou, M.-Z., You, J.-M., and Liang, D.-C. (1987) Refinement of the structure of *des*-pentapetide (B26-B30) insulin at 1.5 Å resolution, *Sci. Sintering 30*, 55−65.
9. Baker, E. N., Blundell, T. L., Cutfield, J. F., Cutfield, S. M., Dodson, E. J., Dodson, G. G., Hodgkin, D. M., Hubbard, R. E., Isaacs, N. W., and Reynolds, C. D. (1988) The structure of 2-Zn pig insulin crystals at 1.5 Å resolution, *Philos. Trans. Royal Soc. London 319*, 369−456.
10. Ciszak, E., and Smith, G. D. (1994) Crystallographic evidence for dual coordination around zinc in the T_3R_3 human insulin hexamer, *Biochemistry 33*, 1512−1517.
11. Bao, S. J., Xie, D. L., Zhang, J. P., Chang, W. R., and Liang, D. C. (1997) Crystal structure of *des*-heptapeptide(B24-B30)insulin at 1.6 Å resolution: implications for receptor binding, *Proc. Natl. Acad. Sci. U.S.A. 94*, 2975−2980.
12. Kitagawa, K., Ogawa, H., Burke, G. T., Chanley, J. D., and Katsoyannis, P. G. (1984) Critical role of the A2 amino acid residue in the biological activity of insulin: [2-glycine-A]- and [2-alanine-A]insulins, *Biochemistry 23*, 1405−1413.
13. Nakagawa, S. H., and Tager, H. S. (1992) Importance of aliphatic side-chain structure at positions 2 and 3 of the insulin A-chain in insulin−receptor interactions, *Biochemistry 31*, 3204−3214.
14. Derewenda, U., Derewenda, Z., Dodson, E. J., Dodson, G. G., Bing, X., and Markussen, J. (1991) X-ray analysis of the single chain B29-A1 peptide-linked insulin molecule. A completely inactive analogue, *J. Mol. Biol. 220*, 425−433.
15. Xu, B., Hua, Q. X., Nakagawa, S. H., Jia, W., Chu, Y. C., Katsoyannis, P. G., and Weiss, M. A. (2002) Chiral mutagensis of insulin's hidden receptor-binding surface: structure of an *allo*-isoleucine^{A2} analogue, *J. Mol. Biol. 316*, 435−441.
16. Weiss, M. A., Hua, Q. X., Lynch, C. S., Frank, B. H., and Shoelson, S. E. (1991) Heteronuclear 2-D NMR studies of an engineered insulin monomer: assignment and characterization of the receptor-binding surface by selective ^{2}H and ^{13}C labeling with application to protein design, *Biochemistry 30*, 7373−7389.
17. Kobayashi, M., Ohgaku, S., Iwasaki, M., Maegawa, H., Shigeta, Y., and Inouye, K. (1982) Supernormal insulin: [D-Phe^{B24}]-insulin with increased affinity for insulin receptors, *Biochem. Biophys. Res. Commun. 107*, 329−336.
18. Mirmira, R. G., and Tager, H. S. (1989) Role of the phenylalanine B24 side chain in directing insulin interaction with its receptor: importance of main-chain conformation, *J. Biol. Chem. 264*, 6349−6354.
19. Diao, J.-S., Wan, Z.-L., Chang, W.-R., and Liang, D.-C. (1997) Structure of monomeric porcine *des*[B1-B2]-*des*-pentapeptide (B26-B30) insulin at 1.65 Å resolution, *Acta Crystallogr. D53*, 507−512.
20. Cosmatos, A., Ferderigos, N., and Katsoyannis, P. G. (1979) Chemical synthesis of [*des*(tetrapeptide B27-30), Tyr(NH_2)26-B] and [*des*(pentapeptide B26-30), Phe(NH_2)25-B] bovine insulins, *Int. J. Protein Res. 14*, 457−471.
21. Fischer, W. H., Saunders, D., Brandenburg, D., Wollmer, A., and Zahn, H. (1985) A shortened insulin with full in vitro potency, *Biol. Chem. Hoppe-Seyler 366*, 521−525.
22. Ludvigsen, S., Olsen, H. B., and Kaarsholm, N. C. (1998) A structural switch in a mutant insulin exposes key residues for receptor binding, *J. Mol. Biol. 279*, 1−7.
23. Brems, D. N., Brown, P. L., Nakagawa, S. H., and Tager, H. S. (1991) The conformational stability and flexibility of insulin with an additional intramolecular cross-link, *J. Biol. Chem. 266*, 1611−1615.
24. Derewenda, U., Derewenda, Z., Dodson, E. J., Dodson, G. G., Reynolds, C. D., Smith, G. D., Sparks, C., and Swenson, D. (1989) Phenol stabilizes more helix in a new symmetrical zinc insulin hexamer, *Nature 338*, 594−596.
25. Liang, D. C., Chang, W. R., and Wan, Z. L. (1994) A proposed interaction model of the insulin molecule with its receptor, *Biophys. Chem. 50*, 63−71.
26. Weiss, M. A., Hua, Q.-X., Jia, W., Chu, Y.-C., Wang, R.-Y., and Katsoyannis, P. G. (2000) Hierarchiacal protein undesign: insulin's intrachain disulfide bridge tethers a recognition α-helix, *Biochemistry 39*, 15429−15440.
27. Kristensen, C., Kjeldsen, T., Wiberg, F. C., Schaffer, L., Hach, M., Havelund, S., Bass, J., Steiner, D. F., and Andersen, A. S. (1997) Alanine scanning mutagenesis of insulin, *J. Biol. Chem. 272*, 12978−12983.
28. Xu, B., Hua, Q. X., Nakagawa, S. H., Jia, W., Chu, Y. C., Katsoyannis, P. G., and Weiss, M. A. (2002) A cavity-forming mutation in insulin induces segmental unfolding of a surrounding α-helix, *Protein Sci. 11*, 104−116.
29. Choi, W. E., Borchardt, D., Kaarsholm, N. C., Brzovic, P. S., and Dunn, M. F. (1996) Spectroscopic evidence for preexisting T- and R-state insulin hexamer conformations, *Proteins 26*, 377−390.
30. Pullen, R. A., Lindsay, D. G., Wood, S. P., Tickle, I. J., Blundell, T. L., Wollmer, A., Krail, G., Brandenburg, D., Zahn, H., Gliemann, J., and Gammeltoft, S. (1976) Receptor-binding region of insulin, *Nature 259*, 369−373.
31. Yip, C. C., and Ottensmeyer, P. (2003) Three-dimensional structural interactions of insulin and its receptor, *J. Biol. Chem. 278*, 27329−27332.
32. Weiss, M. A., Hua, Q.-X., Jia, W., Nakagawa, S. H., Chu, Y.-C., Hu, S.-Q., and Katsoyannis, P. G. (2001) Activities of monomeric insulin analogues at position A8 are uncorrelated with their thermodynamic stabilities, *J. Biol. Chem. 276*, 40018−40024.
33. Brünger, A. T. (1993) Assessment of phase accuracy by cross validation: the free *R* value. Methods and applications, *Acta Crystallogr. D49*, 24−36.
34. Brunger, A. T., Adams, P. D., Clore, G. M., DeLano, W. L., Gros, P., Grosse-Kunstleve, R. W., Jiang, J. S., Kuszewski, J., Nilges, M., Pannu, N. S., Read, R. J., Rice, L. M., Simonson, T., and Warren, G. L. (1998) Crystallography and NMR system: A new software suite for macromolecular structure determination, *Acta Crystallogr. D: Biol. Crystallogr. 54*, 905−921.
35. Jones, T. A., Zou, J. Y., Cowan, S. W., and Kjeldgaard, M. (1991) Improved methods for binding protein models in electron density maps and the location of errors in these models, *Acta Crystallogr. A 47*, 110−119.
36. Laskowski, R. A., Macarthur, M. W., Moss, D. S., and Thornton, J. M. (1993) PROCHECK: a program to check the stereochemical quality of protein structures, *J. Appl. Crystallogr. 26*, 283−291.
37. Brunger, A. T. (1993) *XPLOR Manual*, *Version 3.1*, Yale University Press, New Haven, CT.
38. Sosnick, T. R., Fang, X., and Shelton, V. M. (2000) Application of circular dichroism to study RNA folding transitions, *Methods Enzymol. 317*, 393−409.
39. Pace, C. N., and Shaw, K. L. (2000) Linear extrapolation method of analyzing solvent denaturation curves, *Proteins Suppl. 4*, 1−7.
40. Hua, Q. X., Kochoyan, M., and Weiss, M. A. (1992) Structure and dynamics of *des*-pentapeptide-insulin in solution: the molten-globule hypothesis, *Proc. Natl. Acad. Sci. U.S.A. 89*, 2379−2383.
41. Harbury, P. B., Plecs, J. J., Tidor, B., Alber, T., and Kim, P. S. (1998) High-resolution protein design with backbone freedom, *Science 282*, 1462−1467.
42. Smith, G. D., and Dodson, G. G. (1992) Structure of a rhombohedral R_6 insulin/phenol complex, *Proteins 14*, 401−408.
43. Smith, G. D., and Ciszak, E. (1994) The structure of a complex of hexameric insulin and 4′-hydroxyacetanilide, *Proc. Natl. Acad. Sci. U.S.A. 91*, 8851−8855.
44. Ciszak, E., Beals, J. M., Frank, B. H., Baker, J. C., Carter, N. D., and Smith, G. D. (1995) Role of C-terminal B-chain residues in insulin assembly: the structure of hexameric Lys^{B28}Pro^{B29}-human insulin, *Structure 3*, 615−622.
45. Whittingham, J. L., Chaudhuri, S., Dodson, E. J., Moody, P. C., and Dodson, G. G. (1995) X-ray crystallographic studies on hexameric insulins in the presence of helix-stabilizing agents, thiocyanate, methylparaben, and phenol, *Biochemistry 34*, 15553−15563.
46. Smith, G. D., Pangborn, W. A., and Blessing, R. H. (2001) Phase changes in $T_3R_3^f$ human insulin: temperature or pressure induced? *Acta Crystallogr. D57*, 1091−1100.
47. Dong, J., Wan, Z., Popov, M., Carey, P. R., and Weiss, M. A. (2003) Insulin assembly damps conformational fluctuations: Raman analysis of amide I line widths in native states and fibrils, *J. Mol. Biol. 330*, 431−442.
48. Hua, Q. X., Jia, W., Frank, B. H., and Weiss, M. A. (1993) Comparison of the dynamics of an engineered insulin monomer and dimer by acid-quenched amide proton exchange. Nonlocal

stabilization of interchain hydrogen bonds by dimerization, *J. Mol. Biol. 230*, 387−394.
49. Jacoby, E., Hua, Q. X., Stern, A. S., Frank, B. H., and Weiss, M. A. (1996) Structure and dynamics of a protein assembly. ^{1}H NMR studies of the 36 kDa R_6 insulin hexamer, *J. Mol. Biol. 258*, 136−157.
50. Markussen, J., Jorgensen, K. H., Sorensen, A. R., and Thim, L. (1985) Single chain *des*-(B30) insulin. Intramolecular cross-linking of insulin by trypsin catalyzed transpeptidation, *Int. J. Peptide Protein Res. 26*, 70−77.
51. Ottensmeyer, F. P., Beniac, D. R., Luo, R. Z., and Yip, C. C. (2000) Mechanism of transmembrane signaling: insulin binding and the insulin receptor, *Biochemistry 39*, 12103−12112.
52. Chang, W., Jiang, T., Ren, Z., Wan, Z., Xu, Y., Liang, D.-C., Zhu, S., and Zhang, Y. (1995) The crystal structure of *des*-hexapeptide (B25-B30) insulin at 0.25 nm resolution, *Sci. China, Ser. B: Chem. 38*, 1094−1100.
53. Nakagawa, S. H., Tager, H. S., and Steiner, D. F. (2000) Mutational analysis of invariant valine B12 in insulin: implications for receptor binding, *Biochemistry 39*, 15826−15835.
54. Weiss, M. A., Wan, Z., Zhao, M., Chu, Y.-C., Nakagawa, S. H., Burke, G. T., Jia, W., Hellmich, R., and Katsoyannis, P. G. (2001) Nonstandard insulin design: structure−activity relationships at the periphery of the insulin receptor, *J. Mol. Biol. 315*, 103−111.
55. Hu, S. Q., Burke, G. T., Schwartz, G. P., Ferderigos, N., Ross, J. B., and Katsoyannis, P. G. (1993) Steric requirements at position B12 for high biological activity in insulin, *Biochemistry 32*, 2631−2635.
56. Murray-Rust, J., McLeod, A. N., Blundell, T. L., and Wood, S. P. (1992) Structure and evolution of insulins: implications for receptor binding, *Bioessays 14*, 325−331.
57. Weiss, M. A., Nakagawa, S. H., Jia, W., Xu, B., Hua, Q. X., Chu, Y. C., Wang, R. Y., and Katsoyannis, P. G. (2002) Protein structure and the spandrels of San Marco: insulin's receptor-binding surface is buttressed by an invariant leucine essential for protein stability, *Biochemistry 41*, 809−819.
58. Hua, Q.-X., Chu, Y.-C., Jia, W., Phillips, N. F. B., Wang, R.-Y., Katsoyannis, P. G., and Weiss, M. A. (2002) Mechanism of insulin chain combination. Asymmetric roles of A-chain α-helices in disulfide pairing, *J. Biol. Chem. 277*, 43443−43453.
59. De Meyts, P., Van Obberghen, E., and Roth, J. (1978) Mapping of the residues responsible for the negative cooperativity of the receptor-binding region of insulin, *Nature 273*, 504−509.
60. Nakagawa, S. H., and Tager, H. S. (1991) Implicatons of invariant residue Leu^{B6} in insulin−receptor interactions, *J. Biol. Chem. 266*, 11502−11509.
61. Schaffer, L. (1994) A model for insulin binding to the insulin receptor, *Eur. J. Biochem. 221*, 1127−1132.
62. DiMarchi, R. D., Mayer, J. P., Fan, L., Brems, D. N., Frank, B. H., Green, J. K., Hoffman, J. A., Howey, D. C., Long, H. B., Shaw, W. N., Shields, J. E., Slieker, L. J., Su, K. S. E., Sundell, K. L., and Chance, R. E. (1992) in *Peptides: Proceedings of the Twelfth American Peptide Symposium* (Smith, J. A., and Rivier, J. E., Eds.) pp 26−28, ESCOM Science Publishers B. V., Leiden, The Netherlands.

BI034430O